Lab on a Chip

Microfluidic CODES: A Scalable Multiplexed Electronic Sensor for Orthogonal Detection of Particles in Microfluidic Channels

Journal:	*Lab on a Chip*
Manuscript ID	LC-TIN-02-2016-000209
Article Type:	Technical Innovation
Date Submitted by the Author:	15-Feb-2016
Complete List of Authors:	Liu, Ruxiu; Georgia Institute of Technology, Electrical and Computer Engineering Wang, Ningquan; Georgia Institute of Technology, Electrical and Computer Engineering Kamili, Farhan; Georgia Institute of Technology, Electrical and Computer Engineering Sarioglu, A. Fatih; Georgia Institute of Technology, Electrical and Computer Engineering

Microfluidic CODES: A Scalable Multiplexed Electronic Sensor for Orthogonal Detection of Particles in Microfluidic Channels

Ruxiu Liu[a], Ningquan Wang[a], Farhan Kamili[a], A. Fatih Sarioglu[*abc]

[a] School of Electrical and Computer Engineering, Georgia Institute of Technology, Atlanta, GA 30332, USA. Email: sarioglu@gatech.edu

[b] Institute of Electronics and Nanotechnology, Georgia Institute of Technology, Atlanta, GA 30332, USA

[c] Petit Institute for Bioengineering and Biosciences, Georgia Institute of Technology, Atlanta, GA 30332, USA

Abstract

Numerous biophysical and biochemical assays rely on spatial manipulation of particles/cells as they are processed on lab-on-a-chip devices. Analysis of spatially distributed particles on these devices typically requires microscopy negating the cost and size advantages of microfluidic assays. In this paper we introduce a scalable electronic sensor technology, called microfluidic CODES, that utilizes resistive pulse sensing to orthogonally detect particles in multiple microfluidic channels from a single electrical output. Combining the techniques from telecommunications and microfluidics, we route three coplanar electrodes on a glass substrate to create multiple Coulter counters producing distinct orthogonal digital codes when they detect particles. We specifically design a digital code set using the mathematical principles of Code Division Multiple Access (CDMA) telecommunication networks and can decode signals from different microfluidic channels with >90% accuracy through computation even if these signals overlap. As a proof of principle, we use this technology to detect human ovarian cancer cells in four different microfluidic channels fabricated using soft lithography. Microfluidic CODES offers a simple, all-electronic interface that is well suited to create integrated, low-cost lab-on-a-chip devices for cell or particle based assays in resource-limited settings.

Introduction

Detection and analysis of small particles in liquids are of particular interest in numerous applications ranging from biomedicine to environmental monitoring[1-3]. By spatially tracking particles/cells as they are manipulated on lab-on-a-chip devices (e.g., determining the microfluidic channel they are sorted into or the location on the microfluidic device where they are captured), many biophysical or biochemical assays can be performed [4-10]. To obtain such spatial information however, lab-on-a-chip assays almost always require subsequent microscopic analysis negating the cost and portability benefits of these microfluidic devices. Therefore, a simple integrated sensor that can track particles on a microfluidic chip can enable a new generation of devices with sample-to-answer capability in performing various cellular and molecular assays and will particularly be attractive for point-of-care testing in resource-limited settings.

Among various types of biosensors, Coulter counters allow rapid detection of particles all electronically utilizing a technique called resistive pulse sensing (RPS) [11-13]. In RPS, particles of interest are suspended in an electrolyte and passed through a pore between two electrodes. As each particle displaces the electrolyte in the pore, electrical conduction is reduced temporarily allowing particles to be detected. Enabled by this simple and robust sensing mechanism, Coulter counters are versatile instruments that have been used in analysis of blood cells [14-16], proteins [17-19], DNA molecules [20], viruses [21] and nanoparticles [22]. With the goal of increasing the device throughput, electrical detection of particles in multi-channel microfluidic chips has previously been demonstrated either by allocating a dedicated Coulter counter to each microfluidic channel[23-25] or through multiplexing by electrically driving each microfluidic channel at a distinct frequency[26]. These devices, however, are more complex as they require interfacing with a larger number of electrodes. In addition, the scalability of these devices is limited since number of electrodes to interface increases linearly with the number of microfluidic channels.

Orthogonal detection in multiple microfluidic channels can be achieved in a simple and scalable way if signals from different microfluidic channels can be multiplexed without increasing the number of external connections to the microfluidic chip. For this purpose, our solution is to construct sensors in microfluidic channels such that they each generate distinct signals. RPS signals[27-30] as well as optical signals[31,32] are well suited for this purpose as they can be modulated by engineering the sensor geometry. For example, by micropatterning counter-facing electrodes[27], co-planar electrodes[30] or the microfluidic channel itself [28,29], several groups have used RPS pulse waveforms to increase the sensitivity in detection of small particles flowing through a microfluidic channel. On the other hand, generating truly distinguishable signals to orthogonally detect particles in multiple microfluidic channels without increasing the device complexity requires special consideration in coding, sensor design and device layout.

Here, we report a scalable electronic sensor that utilizes code division multiple access (CDMA)[33], a spread spectrum telecommunications technique, for orthogonal detection of particles in multiple microfluidic channels from a single electrical output. We call this technology microfluidic Coded Orthogonal Detection by Electrical Sensing or microfluidic CODES in short. We use microfabrication techniques to create coplanar electrodes such that particles passing over these electrodes produce bipolar digital codes, similar to the digital codes used in CDMA communication networks to differentiate between cell phone users. These codes are designed to be orthogonal to each other so that they can easily be distinguished through computation even when they overlap. Microfluidic CODES is simple and also scalable; it uses only 3 electrodes and can in theory be adapted to orthogonally detect particles in an arbitrary number of microfluidic channels. As a proof of concept, we created a device with four microfluidic channels (Fig. 1a). Using human ovarian cancer cells in phosphate-buffered saline (PBS) as a model biological system, we demonstrated that individual cells in each microfluidic channel could be uniquely detected.

Design of Orthogonal Digital Codes:

CDMA is a spread spectrum communication technique in which multiple users can simultaneously communicate with a base station while sharing the same transmission channel. In CDMA, users' signals are transmitted at the same time and within the same frequency band, while multiplexing is achieved by modulating the information from each user with a unique digital code called digital spreading code. Digital spreading codes are specifically designed to retrieve information in the presence of interference from other users by using a decoding scheme matched to the encoding digital code.

Designing truly distinguishable digital spreading codes is critical to the success of a CDMA system. Mathematically, the similarity between two discrete digital codes (x and y) is defined by a correlation function given by $R_{xy} = \sum_{i=1}^{n} x_i \cdot y_i$,where n is the number of bits. For optimal performance, the set of CDMA digital spreading codes should be designed to be orthogonal. That is, the correlation between different digital spreading codes (i.e., cross-correlation) is zero, while the correlation of the digital spreading code with itself (i.e., autocorrelation) is maximized.

An important aspect of a CDMA system that affects the design of digital spreading codes is its timing properties, i.e., whether the system is synchronous or asynchronous. Our microfluidic CODES device with digitally coded channels can be considered as an asynchronous CDMA system because cells arrive at microfluidic channels at random times. Therefore, our digital codes should work even when they are misaligned with random phase shifts. While it is not possible to design perfectly orthogonal signals for an asynchronous CDMA system, various quasi-orthogonal digital spreading codes exist[34]. Among these, Gold sequences[35,36] are commonly used to minimize multi-user interference in CDMA communication since they have

both desirable autocorrelation and cross correlation properties. Therefore, in this work, we use Gold sequences to encode microfluidic channels.

We generated four 7-bit long Gold sequences to encode four microfluidic channels in our device. A full review of the mathematical framework to generate Gold sequences is beyond the scope of this paper, we therefore briefly outline our design process: First, we used two linear feedback shift-registers representing two primitive polynomials (x^3+x^2+1 and x^3+x+1) to generate a preferred pair of 7-bit maximal length pseudorandom noise sequences (m-sequences). Second, cyclic shifts of preferred pair of m-sequences (m_1=1001011 and m_2=1110100) were added in mod 2 to generate four distinct Gold codes, specifically g_1=1010110, g_2=0111111, g_3=0100010, g_4=0011000. Finally, we validated Gold sequences by analyzing their autocorrelation and periodic cross-correlation properties.

Design of the Microfluidic Chip

We designed and built a device with four microfluidic channels to demonstrate the microfluidic CODES technology (Fig. 1b). In this device, three coplanar electrodes were micropatterned to create arrays of uniformly spaced 10μm-wide fingers at the floor of each microfluidic channel. Finger-to-finger distance was chosen to be on the order of the size of a cell so that the conduction between each pair is locally modulated as the cells flow over them. Therefore, sequential interaction of each cell with finger electrode pairs in the array generates a series of electrical pulses, which are then used to generate digital codes.

An important advantage of our electrode design is that we can generate bipolar signals. In CDMA, bipolar signals are preferred over unipolar signals, because absence of negative values leads to non-ideal cross-correlation properties[37,38]. Because impedance modulation between two electrodes is inherently unipolar, we place an extra reference electrode in between and use the differential impedance modulation to generate a bipolar signal [14].

With the microfluidic CODES technology, we also introduce a systematic approach that can be adapted to generate any digital code for encoding an arbitrary number of microfluidic channels (Fig. 1b). First, we place positive and negative electrodes on the opposite sides of each microfluidic channel. These electrodes each extend into the microfluidic channel through fingers. For each microfluidic channel, positive and negative fingers are ordered to follow the unique digital code. Second, the reference electrode fingers are placed in between positive and negative electrode fingers. In this configuration, each bit spatially corresponds to center-to-center distance between reference electrode fingers, while the electrode finger in between determines the bit polarity (Fig. 1c). Finally, to minimize undesired conduction in microfluidic channels outside the coding region, we place positive and negative electrode traces far from the outer reference electrode fingers (Fig. 1b).

We also optimize our system to detect differential impedance changes caused by flowing cells with maximum sensitivity. Since our electrodes monitor all microfluidic channels simultaneously, cells flowing in a single microfluidic channel lead to only small changes in the overall impedance. Such small changes can easily be dominated by static differential impedance unless static impedances between the reference and positive/negative electrodes are balanced. To balance the system, we use an equal total number of positive and negative electrode fingers. Therefore, we design a digital code set with an equal total number of 1s and 0s. When balanced this way, our technique is not only more sensitive but also more robust to changes in fluid or material properties.

Besides the electrode layout, design of the microfluidic layer is also critical for proper operation. Unlike a CDMA telecommunication network in which signals are digitally generated based on stable clock signals, temporal properties of our digital codes are determined by flow speeds of individual cells. As such, variations in cell flow speed lead to differences in digital code durations perturbing favorable cross-correlation properties of the designed digital code set. To minimize such variations,

we design our device such that fluid flows at the same rate in all microfluidic channels and remains constant across the coding region. In our device, we achieve this by designing each microfluidic channel with uniform cross sections and with equal hydraulic resistance. In addition, we designed the microfluidic channel cross section to be close to the cell size so that (1) cell speed is less affected by the parabolic flow profile across the microfluidic channel, (2) total sensing volume is minimized to reduce cell overlapping, and (3) cells remain close to the surface electrodes increasing the device sensitivity.

Experimental Methods

Our device is composed of a glass substrate with micropatterned surface electrodes that generate digital codes and a polydimethylsiloxane (PDMS) microfluidic layer. We fabricated our device using conventional microfabrication techniques and soft lithography. We created surface electrodes on a glass wafer using lift-off process. 1.5μm-thick negative photoresist was patterned using optical lithography followed by e-beam deposition of 20nm-thick Cr and 80nm-thick Au film stack. The lift-off process was completed in acetone under mild sonication and the patterned wafer was diced to create individual chips. The microfluidic layer was fabricated using soft lithography. 15μm-thick SU-8 photoresist was patterned on a silicon wafer using optical lithography to fabricate the mold. PDMS prepolymer and crosslinker (Sylgard 184, Dow Corning) were mixed at 10:1 ratio and poured on the mold, degassed and then cured at 65°C for 4 hours. Cured PDMS peeled of from the mold and glass substrate with surface electrodes were activated in oxygen plasma, aligned and bonded to create the final device (Fig. 1b).

As a model biological sample, we used cells suspended in PBS. We cultured HeyA8 ovarian cancer cell line (obtained from Dr. John F. McDonald, Georgia Institute of Technology) in RPMI 1640 (Mediatech; Cellgro, Herndon, VA) supplemented with 10% FBS (Fetal Bovine Serum; Seradigm, Radnor, PA) and 1% penicillin-streptomycin (aMResco, Solon, OH) in 5% CO_2 atmosphere at 37°C until they

reached 80% confluence. Following trypsinization for 2 minutes, cells were pelleted, suspended in PBS and mixed with gentle pipetting to mechanically dissociate any cell clusters.

Our measurement setup consists of a syringe pump for driving the cells through the microfluidic chip, electronic hardware for data acquisition and processing of raw sensor signals, and an optical microscope equipped with a high-speed camera for the visual analysis of cell flow in microfluidic channels (Fig. 2).

We generated digital codes by detecting the changes in the magnitude of electrical current as cells flow through microfluidic channels. For this purpose, we excited the system from the reference electrode with a sine wave at 400kHz, specifically to bypass the double layer capacitances at the electrode-liquid interface. Current flow through negative and positive electrodes was independently measured using two transimpedance amplifiers. These signals were then subtracted from each other using a differential amplifier to obtain a bipolar signal. Specifically, we subtracted the positive electrode signal from the negative electrode signal so that reduced electrical current led to positive peaks in the output. The magnitude of this differential signal was measured using a lock-in amplifier. Lock-in amplifier output was then sampled at 1 MHz into a computer using a data acquisition board to decode digital codes.

Through transparent glass substrate, we optically analyzed cell flow through coding electrodes to validate acquired electrical signals. We imaged the microfluidic chip using an inverted optical microscope (Nikon Eclipse Ti-E) equipped with a high-speed camera (Vision Research Phantom v7.3). We recorded movies of cells at 8000 frames per second so that we could resolve them as they passed through microfluidic channels within milliseconds. The recorded videos were then downloaded onto a computer to be analyzed frame by frame.

Results and Discussion

Digital code signals corresponding to each of the four microfluidic channels are easily identified in the recorded electrical waveform. Measured code signals closely match with the designed digital codes (Fig. 3a). Deviations from ideal square pulses can be attributed to several factors including non-uniform electric field between coplanar electrodes, spherical cell shape, and continuous (i.e., not pulsatile) flow of cells in microfluidic channels.

To decode electrical signals, we first created a template library using experimentally obtained digital codes signals corresponding to each microfluidic channel. The template library included four measured, normalized code signals and their computer generated versions with varying durations to accommodate differences in flow speed between different cells. By correlating the recorded electrical signal with all of the templates in the library, we determined the specific template that maximized the amplitude of the autocorrelation peak. From this template, we obtained (1) the specific microfluidic channel the cell passed through, (2) the digital code signal duration and hence the cell transit time (Fig. 3b). Note that an autocorrelation peak can robustly be identified in this process because the digital codes for each microfluidic channel are designed to be orthogonal to each other. Specifically, peak amplitude of periodic cross-correlation between 7-bit Gold sequences corresponding two different microfluidic channels is bounded and can only be as high as ~40% of the autocorrelation peak theoretically.

An important feature of the microfluidic CODES technology is that it can also resolve cells in microfluidic channels even when multiple cells simultaneously occupy the coding electrodes. When cells overlapped, signals due to different cells interfere and the recorded electrical signal cannot be readily associated with a single template corresponding to a specific microfluidic channel. Resolving such overlapping cells, however, is particularly important for processing samples with high cell density, where cells are more likely to overlap.

To demonstrate how microfluidic CODES can resolve overlapping cells, we present an example that involved four overlapping cells in four different microfluidic channels (Fig. 4). To resolve signals corresponding to individual cells, we developed an iterative approach based on the successive interference cancellation scheme[39] used for multi-user detection in CDMA. First, we determined the dominant autocorrelation peak corresponding to the strongest interfering signal by correlating the recorded waveform with the template library (Fig. 4a, 1st row, 2nd plot). Using the amplitude and time of the autocorrelation peak as well as the template used, we estimated the signal due to this specific cell (Fig. 4a, 1st row, 3rd plot). This estimated signal was then subtracted from the original signal, effectively removing the interference due to the largest cell (Fig. 4a, 2nd row, 1st plot). This process was iterated until the correlation of the template library with the residual signal did not produce a clear autocorrelation peak for any channel (Fig. 4a, 5th row, 2nd plot). Specifically, the process was terminated when none of templates correlated with the normalized residual signal led to a correlation coefficient greater than 0.5. Following termination of the interference cancellation process, we ran an optimization process, where the amplitude and duration of estimated cell signals were refined to produce the best fit with the recorded electrical signal based on least-squares approximation (Fig. 4b). At the end of this optimization process, we determined spatial information (the specific microfluidic channel the cell is in), amplitude of the signal and the timing of each overlapping cell (Fig. 4c). Simultaneously recorded high-speed microscopy confirmed our results showing that microfluidic channels the cells were in and also their timing were correctly determined (Fig. 4d).

Our iterative decoding approach is essential in processing samples containing varying sized particles such as biological samples. Successively canceling interference due to overlapping cells allows us to accurately resolve smaller cells with weaker signals, which are otherwise buried in strong interfering signals from larger cells.

While Fig. 4 demonstrates a case of overlapping cells in different microfluidic channels, it should be noted that cells overlapping within the same microfluidic channel could also be resolved. This is because the overlapping of cells in the same microfluidic channel simply corresponds to interference of the same digital code with its time-shifted form and can successfully be decoded using our approach outlined above.

In addition to discriminating between different microfluidic channels (i.e., spatial information), we also used the amplitude of code waveforms from each microfluidic channel to orthogonally measure cell sizes. To achieve this, we first calibrated measured electrical signals with optically measured cell volume using linear regression (Supplementary Figure 1). Based on this calibration, we used calculated cell signal amplitudes in Fig. 4 to estimate corresponding cell size (Fig. 4c). A comparison of measurements using microfluidic CODES with optically measured cell sizes in Fig. 4 shows that we can accurately determine cell size even for overlapping cells (Table 1).

The timing of cell passage through each microfluidic channel can also be orthogonally determined using microfluidic CODES. This is because Gold sequences (or pseudorandom noise sequences in general) are sensitive to time-shifts and produce sharp autocorrelation peaks at zero time delay. A comparison of our estimates using microfluidic CODES with results obtained from simultaneously recorded high-speed video with a known frame rate shows that time differences between overlapping cells in Fig. 4 can accurately be determined (Table 1).

To demonstrate the performance of our technique over a large number of cells, we processed a model biological sample with a density of $4x10^5$ cells/ml. We analyzed the recorded electrical signal corresponding to more than 1000 cells using Matlab and decoded individual digital codes as follows: Using a low-pass filter, we first removed high frequency noise (>2.5 kHz) in the recorded electrical signal. In the filtered signal, time windows where power of the signal is above a certain threshold

(SNR>12dB) were identified as sensor activity. Each event was then individually analyzed using the iterative algorithm described above. By comparing our results with the simultaneously recorded high-speed microscopy video, we determined that we can identify each cell and the microfluidic channel it passed through with a 96.15% (973/1012) accuracy. In this analysis, success rates for detecting non-overlapping and overlapping cells were 98.71% (688/697) and 90.48% (285/315), respectively. Using calibration parameters (Supplementary Fig. 1), we also measured size and flow speed of cells in our analysis (Fig. 5). Our cell size measurement results match with the optically measured cell size distribution (Supplementary Fig. 2).

Finally, microfluidic CODES can be scaled to incorporate more microfluidic channels. This is achieved by assigning each microfluidic channel a code distinguishable from others. For this purpose, larger digital code sets with favorable correlation properties can be designed by using longer (i.e., more bits) codes. Longer codes are less prone to interference from other codes and can therefore be distinguished from each other with higher accuracy. Furthermore, a key parameter that determines the performance and also the scalability of our sensor is the sample cell density. More microfluidic channels covering a larger sensor area will increase the likelihood of overlapping events and hence the interference. The maximum number of overlapping cells that can be resolved using our technology depends on several factors including the digital code set, the detection algorithm, the design of the microfluidic chip as well as the electronic noise and will ultimately determine the sample cell density that can be processed reliably.

Conclusions

Combining the techniques from telecommunications and microfluidics, we have introduced the microfluidic CODES technology, a scalable electronic sensor to orthogonally detect particles in multiple microfluidic channels from a single electrical output. The microfluidic CODES relies on multiplexing an array of

micromachined Coulter counters each designed to produce a distinct digital code when a particle is detected. These digital codes are developed using the same principles of CDMA telecommunication networks and can be uniquely recovered through simple mathematical calculations. We demonstrated that our technology could readily be applied to detect human ovarian cancer cells on a multi-channel microfluidic chip. Importantly, our technology can also resolve particles with >90% accuracy if they overlap in time, a feature that is required to process samples with high particle density. Microfluidic CODES offers a simple, all-electronic interface for tracking particles on microfluidic devices and is particularly well suited to create integrated, low-cost lab-on-a-chip devices for cell or particle based assays that are needed for point-of-care tests in resource-limited settings.

Acknowledgements

This work was supported by the start-up funds provided to A.F.S by Georgia Institute of Technology, School of Electrical and Computer Engineering. The authors would like to thank Qian Shao for his help in processing sensor signals.

References

1 H. Zhang, C. H. Chon, X. Pan and D. Li, *Microfluidics and Nanofluidics*, 2009, **7**, 739–749.

2 A. Yurt, G. G. Daaboul, J. H. Connor, B. B. Goldberg and M. S. Ünlü, *Nanoscale*, 2012, **4**, 715–726.

3 T. P. Burg, M. Godin, S. M. Knudsen, W. Shen, G. Carlson, J. S. Foster, K. Babcock and S. R. Manalis, *Nature*, 2007, **446**, 1066–1069.

4 L. R. Huang, E. C. Cox, R. H. Austin and J. C. Sturm, *Science*, 2004, **304**, 987-990.

5 G. Wang, W. Mao, R. Byler, K. Patel, C. Henegar, A. Alexeev and T. Sulchek, *PLoS ONE*, 2013, **8**, e75901.

6 E. Ozkumur, A. M. Shah, J. C. Ciciliano, B. L. Emmink, D. T. Miyamoto, E. Brachtel, M. Yu, P. I. Chen, B. Morgan, J. Trautwein, A. Kimura, S. Sengupta, S. L. Stott, N. M. Karabacak, T. A. Barber, J. R. Walsh, K. Smith, P. S. Spuhler, J. P. Sullivan, R. J. Lee, D. T. Ting, X. Luo, A. T. Shaw, A. Bardia, L. V. Sequist, D. N. Louis, S. Maheswaran, R. Kapur, D. A. Haber and M. Toner, *Science Translational Medicine*, 2013, **5**, 179ra47–179ra47.

7 S. Nagrath, L. V. Sequist, S. Maheswaran, D. W. Bell, D. Irimia, L. Ulkus, M. R. Smith, E. L. Kwak, S. Digumarthy, A. Muzikansky, P. Ryan, U. J. Balis, R. G. Tompkins, D. A. Haber and M. Toner, *Nature*, 2007, **450**, 1235-1239.

8 A. F. Sarioglu, N. Aceto, N. Kojic, M. C. Donaldson, M. Zeinali, B. Hamza, A. Engstrom, H. Zhu, T. K. Sundaresan, D. T. Miyamoto, X. Luo, A. Bardia, B. S. Wittner, S. Ramaswamy, T. Shioda, D. T. Ting, S. L. Stott, R. Kapur, S. Maheswaran, D. A. Haber and M. Toner, *Nat. Methods*, 2015, **12**, 685–691.

9 M. E. Warkiani, L. Wu, A. K. P. Tay and J. Han, *Annu Rev Biomed Eng*, 2015, **17**, 1-34.

10 C. W. Shields, C. D. Reyes and G. P. López, *Lab Chip*, 2015, **15**, 1230–1249.

11 R. W. DeBlois and C. P. Bean, *Rev. Sci. Instrum.*, 1970, **41**, 909–916.

12 H. Bayley and C. R. Martin, *Chemical Reviews*, 2000, **100**, 2575–2594.

13 D. Kozak, W. Anderson, R. Vogel and M. Trau, *Nano Today*, 2011, **6**, 531–545.

14 S. Gawad, L. Schild and P. Renaud, *Lab Chip*, 2001, **1**, 76-82

15 D. Holmes, D. Pettigrew, C. H. Reccius, J. D. Gwyer, C. van Berkel, J. Holloway, D. E. Davies and H. Morgan, *Lab Chip*, 2009, **9**, 2881–2889.

16 N. N. Watkins, S. Sridhar, X. Cheng, G. D. Chen, M. Toner, W. Rodriguez and R. Bashir, *Lab Chip*, 2011, **11**, 1437-1447.

17 O. A. Saleh and L. L. Sohn, *Proc. Natl. Acad. Sci. U. S. A.*, 2003, **100**, 820–824.

18 R. Rodriguez-Trujillo, M. A. Ajine, A. Orzan, M. D. Mar, F. Larsen, C. H. Clausen and W. E. Svendsen, *Sens. Actuators A*, 2014, **190**, 922–927.

19 J. Mok, M. N. Mindrinos, R. W. Davis and M. Javanmard, *Proc. Natl. Acad. Sci. U. S. A.*, 2014, **111**, 2110–2115.

20 O. A. Saleh and L. L. Sohn, *Nano Letters*, 2003, **3**, 37–38.

21 R. W. DeBlois and R. K. A. Wesley, *Journal of Virology*, 1977, **23**, 227–233.

22 O. A. Saleh and L. L. Sohn, *Rev. Sci. Instrum.*, 2001, **72**, 4449–4451.

23 J. Zhe, A. Jagtiani, P. Dutta, J. Hu and J. Carletta, *J. Micromech. Microeng.*, 2007, **17**, 304–313.

24 Y. Song, J. Yangi, X. Pan and D. Li, *Electrophoresis*, 2015, **36**, 495–501.

25 Y. Chen, S. J. Kim, J. Guo, Y. Kang and J. P. Kausalya, *Sensors Actuators B*, 2015, **213**, 375-381.

26 A. V. Jagtiani, J. Carletta and J. Zhe, *J. Micromech. Microeng.*, 2011, **21**, 065004.

27 D. Polling, S. C. Deane, M. R. Burcher, C. Glasse and C. H. Reccius, Proceedings of uTAS (The 14th International Conference on Miniaturized Systems for Chemistry and Life Sciences), October 3–7, 2010, Groningen, The Netherlands.

28 M. Javanmard and R. W. Davis, *IEEE Sensors J.*, 2013, **13**, 1399–1400.

29 K. R. Balakrishnan, G. Anwar, M. R. Chapman, T. Nguyen, A. Kesavaraju and L. L. Sohn, *Lab Chip*, 2013, **13**, 1302-1307.

30 S. Emaminejad, S. Talebi, R. W. Davis and M. Javanmard, *IEEE Sensors J.*, 2015, **15**, 2715-2716.

31 P. Kiesel, M. Bassler, M. Beck and N. Johnson, *Appl. Phys. Lett.*, 2009, **94**, 041107

32 J. Martini, M. I. Recht, M. Huck, M. W. Bern, N. M. Johnson and P. Kiesel, *Lab Chip*, 2012, **12**, 5057–5062.

33 D. Torrieri, *Principles of Spread-Spectrum Communication Systems*; Springer: New York, NY, 2015.

34 E. H. Dinan and B. Jabbari, *IEEE Commun. Mag.*, 1998, **36**, 48–54.

35 R. Gold, *IEEE Trans. Inf. Theory*, 1967, **13**, 619–621.

36 R. Gold, *IEEE Trans. Inf. Theory*, 1968, **14**, 154–156.

37 J. A. Salehi, *IEEE Trans. Commun.*, 1989, **37**, 824–833.

38 D. Zaccarin and M. Kavehrad, *J. Lightw. Technol.*, 1994, **12**, 96–105.

39 S. Verdu, *Multiuser Detection*; Cambridge University Press: Cambridge, UK, 1998

Figures

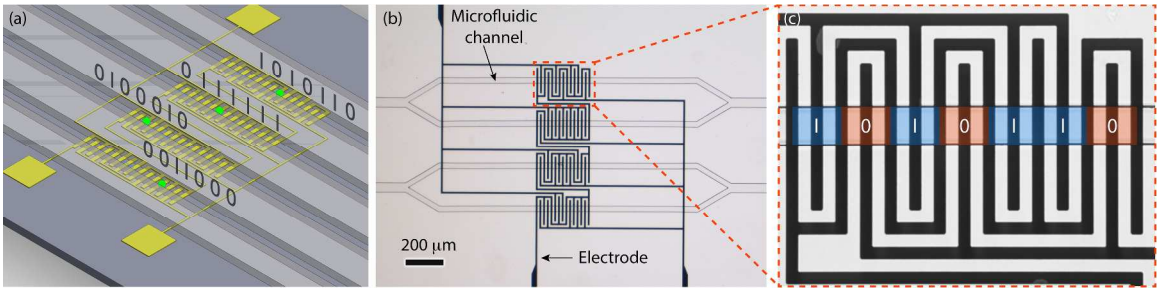

Fig. 1 Design of digitally coded microfluidic channels. (a) Orthogonal digital codes are electrically generated as particles flow over coding surface electrodes. (b) Image of the fabricated device showing coding electrodes on a glass substrate aligned with PDMS microfluidic channels. (c) Close-up of coding electrodes designed to generate the digital code "1010110". Each bit is overlaid on the part of the electrode fingers that generate it.

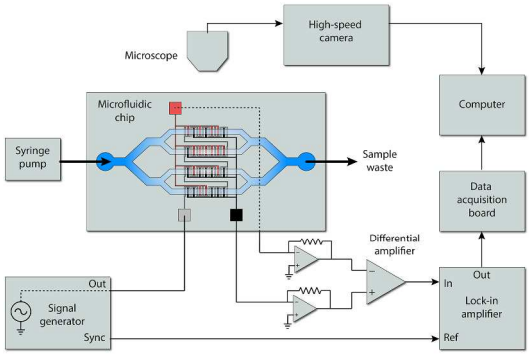

Fig. 2 Experimental setup used for our measurements. Cell suspension is driven through the microfluidic chip using a syringe pump. A bipolar electrical signal is obtained using a differential amplifier and is sampled into a computer for decoding. High-speed optical microscopy is then used to validate decoded electrical signals.

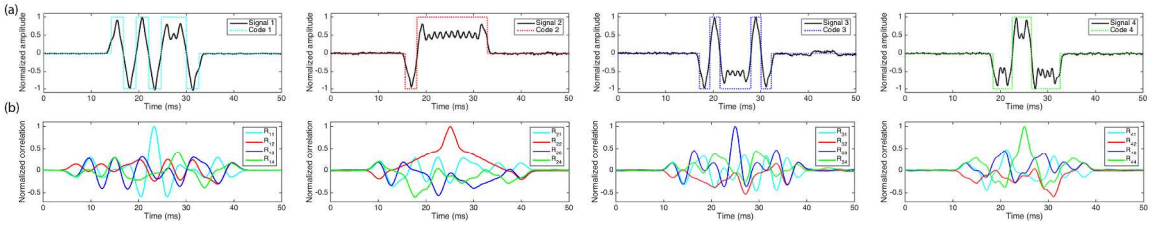

Fig. 3 Measured electrical signals as templates and their correlation. (a) Representative normalized digital code signals (templates) corresponding to each microfluidic channel are shown together with the corresponding ideal square pulse sequences. The signals are recorded as the cells are driven through the microfluidic device at 100 µl/hr. (b) Each template signal is correlated with itself and three other template signals corresponding to other microfluidic channels. In each case, an autocorrelation peak can be identified because the digital codes for each microfluidic channel are specifically designed to be orthogonal to each other.

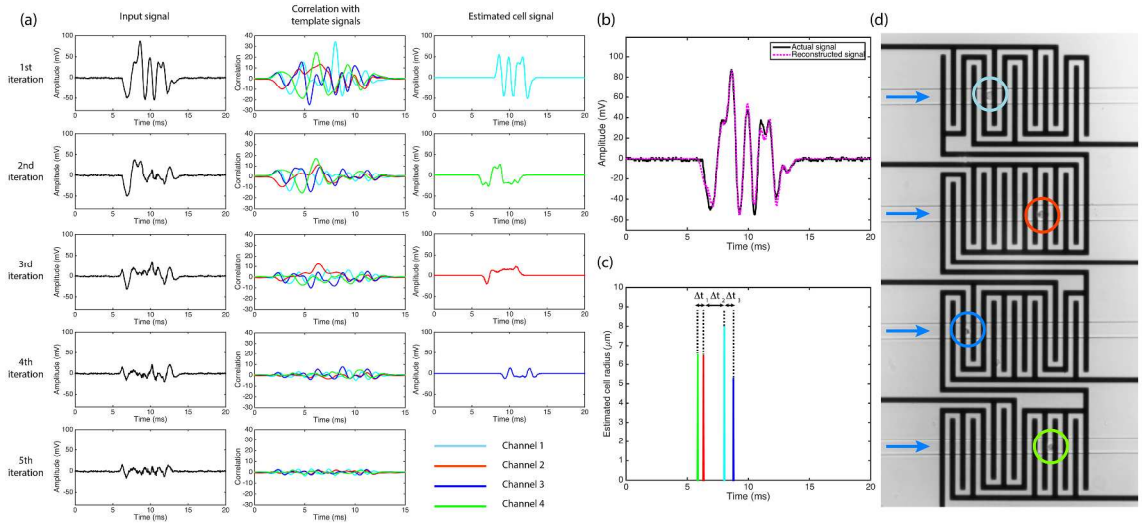

Fig. 4 Decoding the overlapping signals with successive interference cancellation. (a) Input signal (left column) is correlated with the template library to identify the template that leads to maximum correlation amplitude (center column). Using this template as well as the amplitude and time of the correlation peak, signal due to largest overlapping cell is estimated (right column). Estimated signal is then subtracted from the original signal effectively canceling the interference due to the specific cell. The process is repeated until residual signal does not resemble any of the templates in the library (i.e., correlation coefficient < 0.5). (b) Cell signal amplitudes and durations are later optimized to obtain the best fit with the measured signal using least-squares approximation. (c) Optimization process produces accurate results for timing and amplitude of signals (used to compute cell size using calibration data in Supplementary Fig. 1) corresponding to individual cells. (d) Simultaneously recorded high-speed microscopy video confirms the estimated results for location, timing and size of the cells.

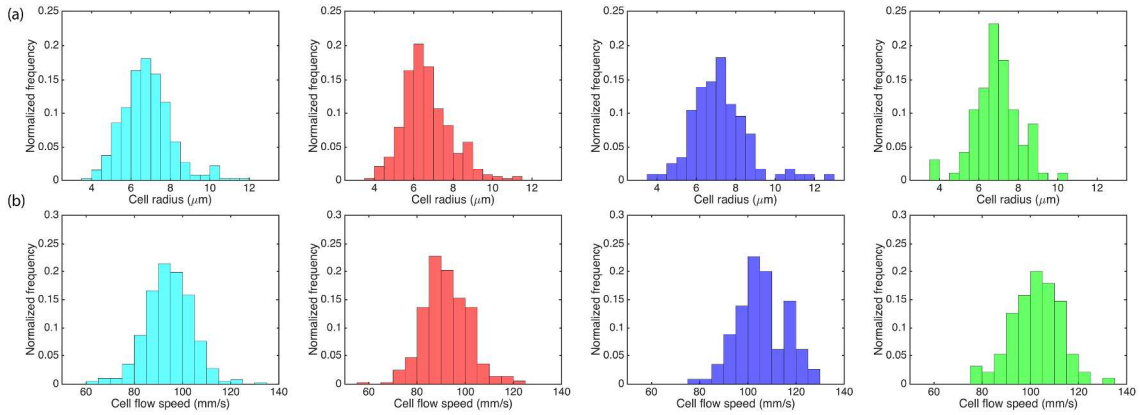

Fig. 5 Orthogonal measurement of cell size and speed in four microfluidic channels. Histograms of calculated cell radius (a) and cell flow speed (b) as the cells are driven at 1000 μl/hr through the microfluidic channels. Recorded electrical waveform is processed using the algorithm outlined in the text. Calculated cell parameters corresponding to microfluidic channel #1 (cyan), #2 (red), #3 (blue) and #4 (green) are grouped in separate histogram plots.

Tables

Table 1 Comparison of electrically and optically measured parameters of Fig. 4c.

Measurement Type	r_{ch1} (μm)	r_{ch2} (μm)	r_{ch3} (μm)	r_{ch4} (μm)	Δt_1 (ms)	Δt_2 (ms)	Δt_3 (ms)
Electrical	8.01	6.49	5.3	6.55	0.465	1.705	0.744
Optical	8.32	6.77	5.68	7.04	0.375	1.625	0.750